Letter

Controllable topological edge mode in an optically excited exciton-polariton lattice

Haochen Wang,[1,*] Hang Zhou,[1,3,*,†] Song Luo,[1,3] Long Zhang,[1,2,‡] and Zhanghai Chen[1,4,5,§]

[1]*Department of Physics, College of Physical Science and Technology, Xiamen University, Xiamen 361005, China*

[2]*State Key Laboratory of Surface Physics and Department of Physics, Fudan University, Shanghai 200433, China*

[3]*Jiujiang Research Institute of Xiamen University, Jiujiang 332000, China*

[4]*Wuhan National High Magnetic Field Center, Wuhan 430074, China*

[5]*Collaborative Innovation Center of Advanced Microstructures, Nanjing University, Nanjing, Jiangsu 210093, China*

(Received 9 June 2022; revised 18 October 2022; accepted 30 November 2022; published 14 December 2022)

We propose an all-optical scheme of topological lasing and switching based on the Aubry-André-Harper (AAH) model of an exciton-polariton chain. We theoretically show that the phase parameter of the optical potential, with a tunable effective quasimomentum, allows the system to exhibit nontrivial topological properties which are attributed to higher dimensions. The topological modes emerging within the bulk band gaps are spatially localized at the edges of the polariton lattice, and their topological properties are characterized by the nonzero Chern numbers of the bulk bands. Polariton lasing in topological edge modes exhibits a higher efficiency and better robustness than in bulk modes, and can be switched between two opposite edges of the lattice by nonresonant excitation, which paves a way for topologically protected optical circuits.

DOI: 10.1103/PhysRevB.106.L220305

The search for novel optical structures to engineer and manipulate the flow of light is a central frontier in photonics. The introduction of topological concepts in recent years has provided a very efficient route for such studies [1,2]. Topologically protected photonic edge states supported at the exteriors of insulating bulk systems are of particular interest, as they enable some unique phenomena, such as robust topological single-mode lasing immune to scattering and disorder [3–5]. The combination of the topological properties and the flexibility of engineering and measuring the band structures in photonic systems underpins potential applications in designing compact, low-loss, and functional photonic chips.

Recently, growing attention has been drawn to introducing some excellent properties of matter into topological photonic structures [6–9]. Among them, microcavity exciton polaritons, quasiparticles arising from the strong coupling between excitons and cavity photons [10], provide unprecedented flexibility to explore topological phenomena [11–26] and to innovate semiconductor topological lasers [27–30]. Benefiting from the hybrid nature, polaritons exhibit lower-threshold single-state condensation, non-Hermitian optical gain and loss, Coulomb interactions, and magnetic responses. By imprinting different lattice potential landscapes, novel phenomena of topological polariton lasing have been proposed, such as the one-dimensional (1D) Su-Schrieffer-Heeger (SSH) model [16,29,30], and two-dimensional (2D) models analogous to quantum Hall [11], quantum spin Hall [19,22], and quantum valley Hall effects [31]. These developments have attracted considerable attention for energy-efficient and scattering-free polariton lasers.

As a further step, accesses to manipulate the topological lasing between distinct states will further enrich the application of topological polariton lasers in optical circuits. In some recent configurations, the propagation direction of a unidirectional topological polariton flow can be reversed, for example, by inverting the magnetic field in a 2D Chern insulator [11], or by inverting the polarization of the circularly polarized pumping at each site in a coupled elliptical micropillar chain [32]. The polarization can also switch a topological phase from nontrivial to trivial in a perovskite zigzag chain, taking advantage of the birefringence of the gain material [33]. These existing schemes require elaborate nanofabrication, a high external magnetic field, or specific material properties, limiting the realization of devices. To achieve topological polariton lasers with the capability of switching, a simple and convenient way, e.g., all-optical operation, is highly desired.

Motivation can be drawn from the realm of condensed matter, where the phase of a periodic lattice can serve as a degree of freedom to manipulate the topological nature. For example, a topological charge pumping scheme called Thouless pumping utilizes the phase of a 1D periodic potential to adiabatically transport an electron gas from one end to the other, similar to the Archimedes screw pumping water via a rotating spiral tube [34–36]. There is a paradigmatic 1D Hamiltonian with an extra phase parameter called the Aubry-André-Harper (AAH) model [37–39], which has diagonal and/or off-diagonal cosinusoidal modulated potentials, and plays an important role in investigating the topological phases and Anderson localization in condensed matter and optics [40]. However, as a versatile quantum simulator, the AAH model has been overlooked in exciton polaritons.

In this Letter, based on the AAH model, we propose an all-optical scheme to implement fast switching of the topological

*These authors contributed equally to this work.
†hangzhou@xmu.edu.cn
‡zhanglong@xmu.edu.cn
§zhanghai@xmu.edu.cn

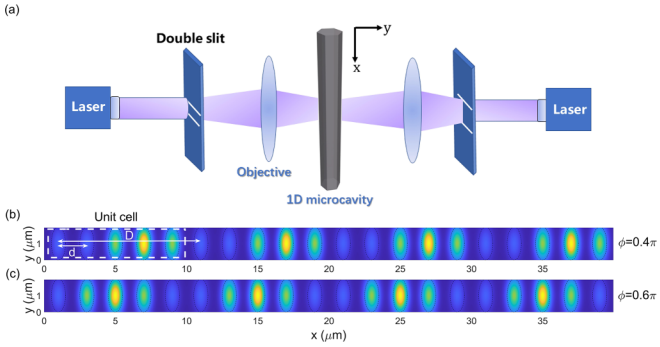

FIG. 1. A 1D polariton lattice generated by optical excitation. (a) Schematic of the experimental setup to generate the optical lattice. Two periodic laser patterns created by two different double slits are shone on the 1D microcavity from the front side and back side, respectively. (b), (c) Spatial distribution of the created laser pattern, which can be described by Eq. (1) with $\phi = 0.40\pi$ and $\phi = 0.60\pi$, respectively. The white dashed rectangle indicates one unit cell of the lattice, where the size of the unit cell and the distance between two sites are described by D and d, respectively. Here, $\lambda = \frac{D}{d} = 5$.

polariton lasing between different edges in a 1D microcavity. The notation "all optical" implies that the potential landscape of polaritons could be fully induced by the optical excitation with a shaped pump laser. By systematically calculating the band structures and eigenstates using a continuum model described by a driven-dissipative Gross-Pitaevskii (GP) equation, we show that the polariton system indeed exhibits edge states that span the band gaps with the varying of the initial phase ϕ in the cosinusoidal modulation. On a fundamental level, the x-dependent phase of the cosinusoidal modulation induces an effective hopping along a synthetic y' direction, which is similar to the threading of magnetic flux through a 2D surface that generates the quantum Hall effect [34], and leads to the topological state located at a single edge with certain ϕ. This is phenomenally similar with the 1D non-Hermitian skin effect, and in contrast with the SSH model where the topological states distribute symmetrically at the two opposite edges. We thus obtain nonzero Chern numbers of bulk bands surrounding the edge modes in a 2D Hamiltonian, which ensure the topological properties of the edge states. One of the key advantages of our results is to implement convenient topological polariton lasers by a nonresonant pump with the capability of ultrafast switching between different edges. The underlying topological properties maintain the power efficiency and robust single-mode nature of the edge-state coherent lasing before and after the switching between different edges, even in the presence of disorder and defects, which is essential for optical circuits and is promising for future polaritonic applications in information processing and quantum computation.

We consider a 1D exciton-polariton lattice depicted schematically in Fig. 1(a), which could be all-optically induced by a shaped nonresonant pump. Specifically, the 1D microcavity is excited from the front side and back side simultaneously by two periodically patterned lasers with different periods. The pattern with a smaller period introduces the lattice sites, which is further modulated by an additional cosinusoidal profile provided by the pattern with a larger period. The pump profile could be generated, for example, by two Young's double slits with different slit widths [41], or by a spatial light modulator [42,43]. The resulting spatial distribution can be described as

$$P(x,y) = \sum_n P_0 \left[\cos^2\left(\frac{\pi}{\lambda} n + \phi\right) + \delta \right] e^{-(\frac{x-x_n}{r_0})^2 - (\frac{y-y_n}{r_0})^2}, \quad (1)$$

where the pump intensity is defined as P_0. We set the dimensionless minimum of the pattern $\delta = 0.11$, and the Gaussian radius $r_0 = 2\ \mu$m. The location of each site is described by the coordinates x_n, y_n. The period of the cosinusoidal modulation λ originates from the ratio of the lattice constants of the two incident periodic laser beams ($\lambda = D/d$). In our calculation, we consider the case of $\lambda = 5$, implying five sites in a unit cell, as indicated by the dashed rectangle in Fig. 1(b). The phase difference between the two optical lattices is described by ϕ. Practically, ϕ can be adiabatically tuned in the range between 0 and π by moving one of the two double slits along the x direction, which shifts the relevant positions of the two periodic patterns. Therefore, the pump profile and its translational symmetry can be continuously manipulated by ϕ. For example, Figs. 1(b) and 1(c) show two different optical lattices with $\phi = 0.40\pi$ and $\phi = 0.60\pi$, which are central asymmetric and symmetric, respectively. Such a beam profile exhibits geometric similarity with the AAH model.

The evolution of the polariton wave function Ψ in the 1D optical lattice can be well described by the driven-dissipative GP equation [44–46]

$$i\hbar \frac{\partial \Psi}{\partial t} = \left[-\frac{\hbar^2 \nabla^2}{2m} + \hbar g_R P + \frac{i\hbar}{2}(RP - \gamma_P) + (g_P - i\alpha)|\Psi|^2 \right] \Psi. \quad (2)$$

Here, the effective mass of the lower polaritons is $m = 1.7 \times 10^{-5} m_e$, with m_e being the free-electron mass. The linear decay rate of polaritons and the nonlinear polariton-polariton interaction strength are denoted as γ_P and g_P, respectively. Physically, the nonresonant optical pump P in Eq. (1) creates an incoherent exciton reservoir and contributes to the polariton dynamics in two aspects: acting as a particle source to compensate losses and providing an effective potential. The prefactors R and g_R quantify the injection rate of polaritons and the optical potential, respectively. They are effective parameters that take into account the contributions of the reservoir excitons, which have the same spatial profile as P. In writing these, we have assumed that the reservoir dynamics is fast, which is relevant to the experiments [41]. In this sense, the excitons are approximated in the steady state, where the exciton depletion due to scattering into the polaritons also reduces the gain process of polaritons, resulting in a dynamic equilibrium of the occupation between the excitonic and polaritonic states. This gain saturation effect introduces an imaginary nonlinearity in the model, where the reservoir-related feedback coefficient is described by α [45]. This simplified GP equation was successfully used to describe polariton condensation in many topological structures, e.g., in an all-optically induced SSH lattice [25] and in a 1D zigzag non-Hermitian chain [32]. To demonstrate the validity of the

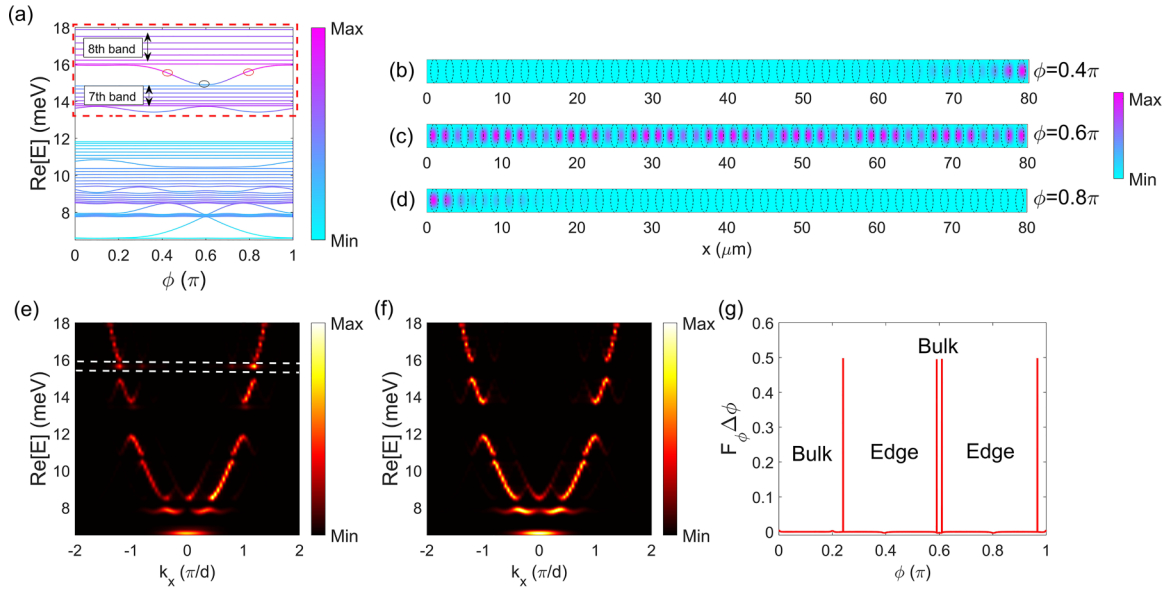

FIG. 2. Band diagram. (a) Band structure of a finite chain under incoherent excitation as a function of ϕ. Each eigenstate of the band is color coded according to the imaginary part with magenta corresponding to the lowest decay and cyan corresponding to the larger decay. (b)–(d) are the real space distributions of the eigenstates labeled by red and black circles in (a), with ϕ of the lattice corresponding to 0.40π, 0.60π, and 0.80π, respectively. Polaritons at states (b) and (d) are spatially localized at the opposite edges of the lattice. In contrast, polaritons at states (c) extend over the lattice. (e) and (f) Energy-resolved momentum-space polariton dispersions with $\phi = 0.40\pi$ and $\phi = 0.60\pi$, respectively. The white dashed lines highlight the edge state emerging in the gap of the bulk bands, whose real space distribution is shown in (b). (g) A parameter defined by Berry curvature in $F_\phi = \frac{1}{2\pi i}\int_{\mathrm{BZ}} dk_x F_{k_x,\phi}$, corresponding to the eighth band in (a), is plotted as a function of ϕ. $P_0 = 90\ \mu\mathrm{m}^{-2}\,\mathrm{ps}^{-1}$, $g_R = 0.080\ \mu\mathrm{m}^2$, $R = 0.059\ \mu\mathrm{m}^2$, and $\gamma_P = 2\ \mathrm{ps}^{-1}$.

above approximations, we show in the Supplemental Material that our results can be reproduced without these approximations by an explicit account of the exciton dynamics [47]. All the parameters used in the following calculations are from the realistic systems.

Before solving the full nonlinear problem, it is instructive to obtain the band structures of linearized modes by neglecting the nonlinear terms in Eq. (2). This treatment is valid provided the regimes of interest are not too far above the condensation threshold, and it fails when the blueshift caused by the interactions exceeds the band gaps. Considering an optical lattice with 40 sites, we use the eigenfunction expansion method to obtain the matrix elements of the Hamiltonian, where the expansion basis vectors are chosen to be sinusoidal to ensure that the wave function Ψ vanishes at the boundaries. The complex energy spectrum E with respect to the phase ϕ is given in Fig. 2(a). Under the modulation of the potential landscape, energy gaps are opened within the bulk bands. In particular, there are modes crossing the gaps. The phase ϕ acts as an effective quasimomentum $k_{y'}$ in a synthetic y' dimension. Accompanied by their nonzero effective group velocities in this synthetic direction, $v_{y'} \sim \partial E/\partial\phi$, these modes exhibit strong spatial localization in the x direction, either at the left or at the right edge of the lattice. For example, the two states of $\phi = 0.40\pi$ and $\phi = 0.80\pi$, labeled by the two red circles in Fig. 2(a), have negative and positive effective group velocities, respectively, corresponding to the right and left edge states, as shown in Figs. 2(b) and 2(d). In contrast, when $\phi = 0.60\pi$ with $v_{y'} = 0$, the wave function of the corresponding eigenstate labeled by the black circle in Fig. 2(a), extends over the lattice, as shown by Fig. 2(c).

To provide better guidance for future experiments, we further investigate the momentum-space dispersion of the modes by Fourier transforming the eigenstates, which can be measured by angle-resolved reflectance or photoluminescence spectroscopy. The momentum-space spectra of the states with $\phi = 0.40\pi$ and $\phi = 0.60\pi$ are plotted in Figs. 2(e) and 2(f), respectively. Both spectra show band folding at the boundaries of mini Brillouin zones, where the band gaps are open. Especially, distinct edge modes emerge within the energy gaps in Fig. 2(e), as indicated by the white dashed lines.

Next, we explore the topological origin of those edge modes. We utilize a discrete manifold method [48] to calculate the Berry curvature and Chern number in the k_x-ϕ space under periodic boundary conditions. This efficient geometrical technique could give integer-valued Chern numbers with high accuracy in any gauge, and requires only a coarse discretization of the Brillouin zone. The Berry curvature is defined as $F_{k_x,\phi} = \partial_{k_x} A_\phi - \partial_\phi A_{k_x}$, where $A_\mu(k_x, \phi)$ is the Berry connection given by $A_\mu(k_x, \phi) = \langle \Psi^a(k_x, \phi)|\partial_\mu|\Psi^b(k_x, \phi)\rangle$, with $\mu = k_x, \phi$. Due to the non-Hermiticity of our system, the superscripts a and b could indicate the right (r) or left (l) eigenvectors of the Hamiltonian, and we find that the following discussion does not depend on the selection of the basis vectors. In order to investigate the ϕ dependence of the Berry curvature, we integrate $F_{k_x,\phi}$ along the k_x direction, and define $F_\phi = \frac{1}{2\pi i}\int_{\mathrm{BZ}} dk_x F_{k_x,\phi}$, with BZ denoting the first Brillouin zone. $F_\phi \Delta\phi$ for the eighth band as a function of ϕ is plotted in Fig. 2(g). Four singular peaks appear at particular values of ϕ, which is analogous to the magnetic monopoles emerging at the Dirac points in the 2D quantum Hall model [38,49,50].

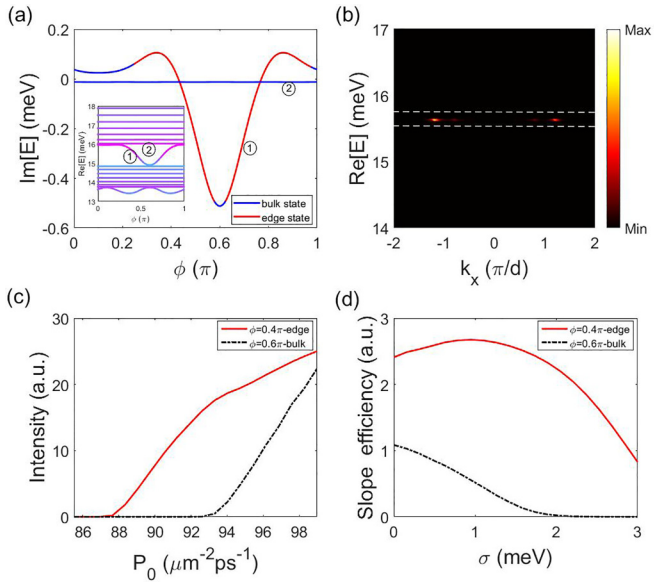

FIG. 3. (a) The solid lines show imaginary parts of the eigenstate as a function of ϕ. The two solid lines labeled by different digit numbers correspond to two energy branches from the band structure (inset). To further distinguish their spatial distribution, edge states and bulk states in each energy branch are plotted in red and blue, respectively. (b) With $\phi = 0.40\pi$ and pump power slightly higher than the threshold, $P_0 = 1.02P_{\text{th}}$, polaritons condensate at the topological edge state, labeled by the white dashed lines. (c) The spectrum intensity as a function of P_0 for the edge and bulk lasing modes. (d) Slope efficiency as a function of disorder strength (measured in terms of the standard deviation) for the edge and bulk lasing modes. Parameters: $g_P = 0.0044$ meV μm^2, $\alpha = 0.05$ meV μm^2. The disorder potential has an isotropic correlation length of 0.12 μm. All other parameters are same as those in Fig. 2.

Then, the Chern number can be obtained as

$$C_n = \frac{1}{2\pi i}\int_0^{\pi} d\phi \int_{\text{BZ}} dk_x F_{k_x,\phi}. \tag{3}$$

The Chern number of the selected bands as labeled by double-arrowed black lines in Fig. 2(a) are $C_{8\text{th}} = 2$ and $C_{7\text{th}} = -1$, respectively. Accordingly, the extracted nonzero topological invariants indicate that the edge states emerging within the bulk band gap are topologically protected.

As a natural driven-dissipative system, polaritons preferentially lase on the states with the largest gain. In the low-density regime, the gain and loss nature of our system is determined by the competition between the spatially inhomogeneous pumping and the intrinsic radiative decay, as reflected in the $RP(x, y)$ and γ_P terms of Eq. (2). The inset of Fig. 3(a) shows two selected bands in Fig. 2(a) labeled by the red dashed rectangle, where the imaginary part of the energy of each state is color coded, with magenta corresponding to the lowest decay and cyan corresponding to the larger decay. The two bands with the largest imaginary components of the system, labeled by 1 and 2, are located in this region, and their imaginary parts are explicitly plotted in Fig. 3(a). According to Fig. 2(g), the interface of the bulk and edge states in the topologically nontrivial band 1 can be determined by the positions of the singular points of $F_\phi \Delta\phi$. The localized edge states of topological origin are in the range of $\phi \in [0.24\pi, 0.59\pi] \cup [0.61\pi, 0.97\pi]$, as coded by red in Fig. 3(a). Compared with the bulk band 2, the edge modes in 1 are found to have a larger gain in the range of $\phi \in [0.24\pi, 0.42\pi) \cup (0.78\pi, 0.97\pi]$, meaning that they would be preferentially selected during polariton lasing. Note that not all the edge states labeled in red can lase spontaneously. Edge-state lasing requires that the polariton wave packets in localized edge states obtain a higher overlap with the pumping spots than that in extended states. Indeed, it is the combination of the non-Hermitian and the topological properties that allows the topologically protected edge states to acquire the largest gain.

Considering the nonlinear repulsive interactions, polaritons in bulk states can be expelled away from the pumping spots, resulting in a larger decay and thus are more difficult to lase in these states. In contrast, the localized states cannot be expelled and thus exhibit a higher gain. We solve Eq. (2) numerically using the time-splitting sine pseudospectral method [51]. In Fig. 3(b), we show polariton lasing at the topological edge state in the momentum space under nonresonant pumping with $\phi = 0.40\pi$. Compared with Fig. 2(e), polaritons accumulate only on a single state and the intensity of the occupied state is five times higher, marking the spontaneous formation of topological condensation. The blueshift induced by the nonlinearity is about 0.02 meV, which is smaller than the band gap $\Delta E_{7\to 8} \simeq 1.19$ meV and does not change the topological properties of the system. For the all-optical scheme we proposed, increasing the pump intensities will bring greater gain and a deeper lattice potential to the system, possibly changing the band structure. We show in Fig. 3(c) the pump-power dependence of the spectrum intensities of the lasing modes at $\phi = 0.40\pi$ and $\phi = 0.60\pi$. The edge-state lasing exhibits a lower threshold and a higher output intensity. When the pump power is higher than the shown range, lasing occurs in both the bulk and edge states due to the enlarged gain. Moreover, we investigate the efficiency and the robustness of the lasing modes in the presence of static disorder in Fig. 3(d) by the power slope efficiency, which is defined as the derivative of the emitted lasing intensity with respect to the input pump power [3]. Significantly, the slope efficiency of edge lasing is higher than that of bulk lasing, and remains high even at strong disorder levels. Interestingly, the slope efficiency of the edge lasing exhibits an enhancement at intermediate values of the disorder strength. A similar phenomenon has been reported in the temporal coherence of a different topological laser model, and has been tentatively explained as an effective suppression of the nonlinear effects in a specific long-wavelength dynamics of the phase by disorder [4].

In Fig. 4, we show the spontaneous formation of the topological polariton lasing at an edge state under nonresonant pumping and the optical switching between different edges. The initial value of ϕ is 0.40π, and the initial wave function of the polariton is Gaussian white noise as shown in Fig. 4(c). With time evolution, polaritons condense at the right edge of the lattice, as indicated in Fig. 4(d), and the system reaches quasiequilibrium. At $T = 150$ ps, the tunable parameter of nonresonant pump ϕ is abruptly switched to 0.80π within the timescale of 10 ps. In the following time, the condensates evolve to the left edge, as indicated by the red solid

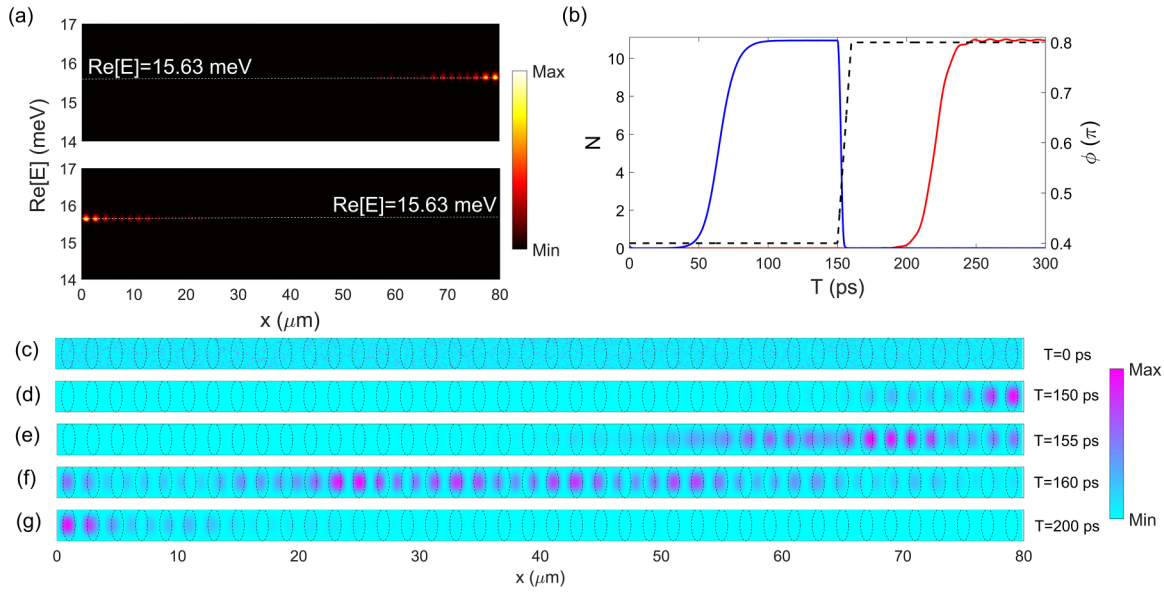

FIG. 4. (a) Polariton condensates in real space with $\phi = 0.40\pi$ (top panel) and $\phi = 0.80\pi$ (bottom panel). (b) Time evolution of polariton condensates at the left edge (red solid line) and right edge (blue solid line) when ϕ is tuned from 0.40π to 0.80π (black dashed line). (c)–(g) Real space distribution of the polaritons at selected moments in (b), illustrating that the location of polariton condensates is switched from the right to the left edge. The pump power is fixed at $P_0 = 90$ meV μm^2, and other parameters are the same as those in Fig. 3.

line in Fig. 4(b). Figures 4(e) and 4(f) selectively show the wave-function distribution at two different moments. Eventually, the exciton-polariton condenses stably at the left edge state. Such a transportation process of polariton lasing is completed in less than 50 ps. This all-optical scheme provides us with the potential applications for optical circuit devices that switch between two different topological edge states.

In conclusion, we have presented a scheme to obtain topological polariton lasing by an all-optical method. The phase of the optical lattice can serve as a new degree of freedom to tune the system from trivial bulk states to nontrivial topological edge states. The translational symmetry breaking of the lattice, together with the non-Hermitian optical control, makes topological polariton condensates switchable between the opposite edges. Given its topological nature and flexible tunability, such a chain can be extremely useful in future polaritonic circuits and can also be integrated as a controllable laser in optical networks. These results are suitable for the exciton polariton with a low optically induced potential. This proposal can be readily applied to room-temperature polariton systems such as ZnO [41,52–54], GaN [55], organics [56,57], and perovskites [58].

The work is supported by the National Key R&D Program of China (Grant No. 2018YFA0306304), the National Natural Science Foundation of China (Grants No. 91950201, No. 62175207, and No. 11674069), State Key Laboratory of Surface Physics and Department of Physics at Fudan University (KF202106), the Interdisciplinary program of Wuhan National High Magnetic Field Center (Grant No. WHMFC202111), Huazhong University of Science and Technology, and Fundamental Research Funds for the Central Universities (20720210004, 20720200074). The authors are grateful to T. Zeng, Y. Li, and X. Lu for fruitful discussions.

[1] L. Lu, J. D. Joannopoulos, and M. Soljačić, Topological photonics, Nat. Photon. **8**, 821 (2014).
[2] T. Ozawa, H. M. Price, A. Amo, N. Goldman, M. Hafezi, L. Lu, M. C. Rechtsman, D. Schuster, J. Simon, O. Zilberberg, and I. Carusotto, Topological photonics, Rev. Mod. Phys. **91**, 015006 (2019).
[3] G. Harari, M. A. Bandres, Y. Lumer, M. C. Rechtsman, Y. D. Chong, M. Khajavikhan, D. N. Christodoulides, and M. Segev, Topological insulator laser: Theory, Science **359**, eaar4003 (2018).
[4] I. Amelio and I. Carusotto, Theory of the Coherence of Topological Lasers, Phys. Rev. X **10**, 041060 (2020).
[5] M. Seclì, M. Capone, and I. Carusotto, Theory of chiral edge state lasing in a two-dimensional topological system, Phys. Rev. Res. **1**, 033148 (2019).
[6] J. Cao, A. V. Kavokin, and A. V. Nalitov, Tamm states and gap topological numbers in photonic crystals, PIER **173**, 141 (2022).
[7] E. Sedov, M. Glazov, and A. Kavokin, Spin-Selective Currents of Tamm Polaritons, Phys. Rev. Appl. **17**, 024037 (2022).
[8] J. C. G. Henriques, T. G. Rappoport, Y. V. Bludov, M. I. Vasilevskiy, and N. M. R. Peres, Topological photonic Tamm states and the Su-Schrieffer-Heeger model, Phys. Rev. A **101**, 043811 (2020).
[9] T. S. Zeng, Fractional quantum Hall effect of Bose-Fermi mixtures, Phys. Rev. B **103**, L201118 (2021).
[10] H. Deng, H. Haug, and Y. Yamamoto, Exciton-polariton Bose-Einstein condensation, Rev. Mod. Phys. **82**, 1489 (2010).
[11] S. Klembt, T. H. Harder, O. A. Egorov, K. Winkler, R. Ge, M. A. Bandres, M. Emmerling, L. Worschech, T. C. Liew,

M. Segev, C. Schneider, and S. Höfling, Exciton-polariton topological insulator, Nature (London) **562**, 552 (2018).

[12] D. D. Solnyshkov, G. Malpuech, P. St-Jean, S. Ravets, J. Bloch, and A. Amo, Microcavity polaritons for topological photonics [Invited], Opt. Mater. Express **11**, 1119 (2021).

[13] T. Karzig, C. E. Bardyn, N. H. Lindner, and G. Refael, Topological Polaritons, Phys. Rev. X **5**, 031001 (2015).

[14] L. Pickup, H. Sigurdsson, J. Ruostekoski, and P. G. Lagoudakis, Synthetic band-structure engineering in polariton crystals with non-Hermitian topological phases, Nat. Commun. **11**, 4431 (2020).

[15] R. Banerjee, T. C. H. Liew, and O. Kyriienko, Realization of Hofstadter's butterfly and a one-way edge mode in a polaritonic system, Phys. Rev. B **98**, 075412 (2018).

[16] P. St-Jean, V. Goblot, E. Galopin, A. Lemaître, T. Ozawa, L. L. Gratiet, I. Sagnes, J. Bloch, and A. Amo, Lasing in topological edge states of a one-dimensional lattice, Nat. Photon. **11**, 651 (2017).

[17] C. Zhang, Y. Wang, and W. Zhang, Topological phase transition with p orbitals in the exciton-polariton honeycomb lattice, J. Phys.: Condens. Matter **31**, 335403 (2019).

[18] A. V. Nalitov, D. D. Solnyshkov, and G. Malpuech, Polariton $\mathbb{Z}$ Topological Insulator, Phys. Rev. Lett. **114**, 116401 (2015).

[19] M. Li, I. Sinev, F. Benimetskiy, T. Ivanova, E. Khestanova, S. Kiriushechkina, A. Vakulenko, S. Guddala, M. Skolnick, V. M. Menon, D. Krizhanovskii, A. Alù, A. Samusev, and A. B. Khanikaev, Experimental observation of topological Z_2 exciton-polaritons in transition metal dichalcogenide monolayers, Nat. Commun. **12**, 4425 (2021).

[20] A. Janot, B. Rosenow, and G. Refael, Topological polaritons in a quantum spin Hall cavity, Phys. Rev. B **93**, 161111(R) (2016).

[21] B. Bahari, A. Ndao, F. Vallini, A. E. Amili, Y. Fainman, and B. Kant, Nonreciprocal lasing in topological cavities of arbitrary geometries, Science **358**, 636 (2017).

[22] W. Liu, Z. Ji, Y. Wang, G. Modi, M. Hwang, B. Zheng, V. J. Sorger, A. Pan, and R. Agarwal, Generation of helical topological exciton-polaritons, Science **370**, 600 (2020).

[23] F. Baboux, E. Levy, A. Lemaître, C. Gómez, E. Galopin, L. Le Gratiet, I. Sagnes, A. Amo, J. Bloch, and E. Akkermans, Measuring topological invariants from generalized edge states in polaritonic quasicrystals, Phys. Rev. B **95**, 161114(R) (2017).

[24] W. Gao, X. Li, M. Bamba, and J. Kono, Continuous transition between weak and ultrastrong coupling through exceptional points in carbon nanotube microcavity exciton-polaritons, Nat. Photon. **12**, 362 (2018).

[25] M. Pieczarka, E. Estrecho, S. Ghosh, M. Wurdack, M. Steger, D. W. Snoke, K. West, L. N. Pfeiffer, T. C. H. Liew, A. G. Truscott, and E. A. Ostrovskaya, Topological phase transition in an all-optical exciton-polariton lattice, Optica **8**, 1084 (2021).

[26] S. Alyatkin, H. Sigurdsson, A. Askitopoulos, J. D. Töpfer, and P. G. Lagoudakis, Quantum fluids of light in all-optical scatterer lattices, Nat. Commun. **12**, 5571 (2021).

[27] Y. V. Kartashov and D. V. Skryabin, Two-Dimensional Topological Polariton Laser, Phys. Rev. Lett. **122**, 083902 (2019).

[28] D. Smirnova, D. Leykam, Y. Chong, and Y. Kivshar, Nonlinear topological photonics, Appl. Phys. Rev. **7**, 021306 (2020).

[29] M. Dusel, S. Betzold, T. H. Harder, M. Emmerling, J. Beierlein, J. Ohmer, U. Fischer, R. Thomale, C. Schneider, S. Höfling, and S. Klembt, Room-temperature topological polariton laser in an organic lattice, Nano Lett. **21**, 6398 (2021).

[30] T. H. Harder, M. Sun, O. A. Egorov, I. Vakulchyk, J. Beierlein, P. Gagel, M. Emmerling, C. Schneider, U. Peschel, I. G. Savenko, S. Klembt, and S. Höfling, Coherent topological polariton laser, ACS Photon. **8**, 1377 (2021).

[31] R. Banerjee, S. Mandal, and T. C. H. Liew, Optically induced topological spin-valley Hall effect for exciton polaritons, Phys. Rev. B **103**, L201406 (2021).

[32] S. Mandal, R. Banerjee, E. A. Ostrovskaya, and T. C. H. Liew, Nonreciprocal Transport of Exciton Polaritons in a Non-Hermitian Chain, Phys. Rev. Lett. **125**, 123902 (2020).

[33] R. Su, S. Ghosh, T. C. Liew, and Q. Xiong, Optical switching of topological phase in a perovskite polariton lattice, Sci. Adv. **7**, 1 (2021).

[34] Y. E. Kraus, Y. Lahini, Z. Ringel, M. Verbin, and O. Zilberberg, Topological States and Adiabatic Pumping in Quasicrystals, Phys. Rev. Lett. **109**, 106402 (2012).

[35] S. Nakajima, T. Tomita, S. Taie, T. Ichinose, H. Ozawa, L. Wang, M. Troyer, and Y. Takahashi, Topological Thouless pumping of ultracold fermions, Nat. Phys. **12**, 296 (2016).

[36] M. Lohse, C. Schweizer, O. Zilberberg, M. Aidelsburger, and I. Bloch, A Thouless quantum pump with ultracold bosonic atoms in an optical superlattice, Nat. Phys. **12**, 350 (2016).

[37] Y. Ke, X. Qin, F. Mei, H. Zhong, Y. S. Kivshar, and C. Lee, Topological phase transitions and Thouless pumping of light in photonic waveguide arrays, Laser Photon. Rev. **10**, 995 (2016).

[38] S. Ganeshan, K. Sun, and S. Das Sarma, Topological Zero-Energy Modes in Gapless Commensurate Aubry-André-Harper Models, Phys. Rev. Lett. **110**, 180403 (2013).

[39] Q.-B. Zeng, Y.-B. Yang, and Y. Xu, Topological phases in non-Hermitian Aubry-André-Harper models, Phys. Rev. B **101**, 020201(R) (2020).

[40] F. Wang, B. Liu, G. Lei, Y. Li, Z. Qi, and C. Qin, Topological edge modes and localization transition in quasiperiodic graphene multilayer arrays, Opt. Laser Technol. **152**, 107957 (2022).

[41] S. Luo, L. Liao, Z. Zhang, J. Wang, X. Shen, and Z. Chen, Classical Spin Chains Mimicked by Room-Temperature Polariton Condensates, Phys. Rev. Appl. **13**, 044052 (2020).

[42] O. Bleu, D. D. Solnyshkov, and G. Malpuech, Full optical control of topological transitions in polariton Chern insulator analog, arXiv:1606.07410.

[43] N. G. Berloff, M. Silva, K. Kalinin, A. Askitopoulos, J. D. Töpfer, P. Cilibrizzi, W. Langbein, and P. G. Lagoudakis, Realizing the classical XY Hamiltonian in polariton simulators, Nat. Mater. **16**, 1120 (2017).

[44] M. Wouters and I. Carusotto, Excitations in a Nonequilibrium Bose-Einstein Condensate of Exciton Polaritons, Phys. Rev. Lett. **99**, 140402 (2007).

[45] M. O. Borgh, J. Keeling, and N. G. Berloff, Spatial pattern formation and polarization dynamics of a nonequilibrium spinor polariton condensate, Phys. Rev. B **81**, 235302 (2010).

[46] J. Keeling and N. G. Berloff, Spontaneous Rotating Vortex Lattices in a Pumped Decaying Condensate, Phys. Rev. Lett. **100**, 250401 (2008).

[47] See Supplemental Material at http://link.aps.org/supplemental/10.1103/PhysRevB.106.L220305 for additional details on (i) calculation of band structures of the polariton chain, (ii) effect of the reservoir dynamics, and (iii) lasing and switching under disorder and defects.

[48] T. Fukui, Y. Hatsugai, and H. Suzuki, Chern numbers in discretized Brillouin zone: Efficient method of computing (spin) Hall conductances, J. Phys. Soc. Jpn. **74**, 1674 (2005).

[49] N. R. Cooper, J. Dalibard, and I. B. Spielman, Topological bands for ultracold atoms, Rev. Mod. Phys. **91**, 015005 (2019).

[50] F. Liu, S. Ghosh, and Y. D. Chong, Localization and adiabatic pumping in a generalized Aubry-André-Harper model, Phys. Rev. B **91**, 014108 (2015).

[51] X. Antoine, W. Bao, and C. Besse, Computational methods for the dynamics of the nonlinear Schrödinger/Gross-Pitaevskii equations, Comput. Phys. Commun. **184**, 2621 (2013).

[52] L. Sun, Z. Chen, Q. Ren, K. Yu, L. Bai, W. Zhou, H. Xiong, Z. Q. Zhu, and X. Shen, Direct Observation of Whispering Gallery Mode Polaritons and their Dispersion in a ZnO Tapered Microcavity, Phys. Rev. Lett. **100**, 156403 (2008).

[53] W. Xie, H. Dong, S. Zhang, L. Sun, W. Zhou, Y. Ling, J. Lu, X. Shen, and Z. Chen, Room-Temperature Polariton Parametric Scattering Driven by a One-Dimensional Polariton Condensate, Phys. Rev. Lett. **108**, 166401 (2012).

[54] F. Li, L. Orosz, O. Kamoun, S. Bouchoule, C. Brimont, P. Disseix, T. Guillet, X. Lafosse, M. Leroux, J. Leymarie, M. Mexis, M. Mihailovic, G. Patriarche, F. Réveret, D. Solnyshkov, J. Zuniga-Perez, and G. Malpuech, From Excitonic to Photonic Polariton Condensate in a ZnO-Based Microcavity, Phys. Rev. Lett. **110**, 196406 (2013).

[55] G. Malpuech, A. Di Carlo, A. Kavokin, J. J. Baumberg, M. Zamfirescu, and P. Lugli, Room-temperature polariton lasers based on GaN microcavities, Appl. Phys. Lett. **81**, 412 (2002).

[56] S. Kéna-Cohen and S. R. Forrest, Room-temperature polariton lasing in an organic single-crystal microcavity, Nat. Photon. **4**, 371 (2010).

[57] G. Lerario, A. Fieramosca, F. Barachati, D. Ballarini, K. S. Daskalakis, L. Dominici, M. De Giorgi, S. A. Maier, G. Gigli, S. Kéna-Cohen, and D. Sanvitto, Room-temperature superfluidity in a polariton condensate, Nat. Phys. **13**, 837 (2017).

[58] R. Su, C. Diederichs, J. Wang, T. C. Liew, J. Zhao, S. Liu, W. Xu, Z. Chen, and Q. Xiong, Room-temperature polariton lasing in all-inorganic perovskite nanoplatelets, Nano Lett. **17**, 3982 (2017).